

# *Ab initio* wavefunction analysis of electron removal quasi-particle state of NdNiO<sub>2</sub> with fully correlated quantum chemical methods

Vamshi M. Katukuri,<sup>1,\*</sup> Nikolay A. Bogdanov,<sup>1</sup> and Ali Alavi<sup>1,2,†</sup>

<sup>1</sup>*Max Planck Institute for Solid State Research, Heisenbergstrasse 1, 70569 Stuttgart, Germany*

<sup>2</sup>*Department of Chemistry, University of Cambridge, Lensfield Road, Cambridge CB2 1EW, UK*

(Dated: January 17, 2022)

The discovery of superconductivity in hole-doped infinite-layer NdNiO<sub>2</sub> — a transition metal (TM) oxide that is both isostructural and isoelectronic to cuprate superconductors — has lead to renewed enthusiasm in the hope of understanding the origin of unconventional superconductivity. Here, we investigate the electron-removal states in infinite-layered Ni<sup>1+</sup> oxide, NdNiO<sub>2</sub>, which mimics hole-doping, with the state-of-the-art many-body multireference quantum chemistry methods. From the analysis of the many-body wavefunction we find that the hole-doped  $d^8$  ground state of NdNiO<sub>2</sub> is very different from the  $d^8$  ground state in isostructural cuprate analog CaCuO<sub>2</sub>, although the parent  $d^9$  ground states are for the most part identical. We show that the doped hole in NdNiO<sub>2</sub> mainly localizes on the Ni  $3d_{x^2-y^2}$  orbital to form a closed-shell singlet, and this singlet configuration contributes to  $\sim 40\%$  of the wavefunction. In contrast, in CaCuO<sub>2</sub> the Zhang-Rice singlet configurations contribute to  $\sim 65\%$  of the wavefunction. With the help of the quantum information concept of entanglement entropy, we quantify the different types of electronic correlations in the nickelate and cuprate compounds, and find that the dynamic radial-type correlations within the Ni  $d$  manifold are persistent in hole-doped NdNiO<sub>2</sub>. As a result, the  $d^8$  multiplet effects are stronger and the additional hole foot-print is more three dimensional in NdNiO<sub>2</sub>. Our analysis shows that the most commonly used three-band Hubbard model employed to express the doped scenario in cuprates represents  $\sim 90\%$  of the  $d^8$  wavefunction for CaCuO<sub>2</sub>, but such a model grossly approximates the  $d^8$  wavefunction for NdNiO<sub>2</sub> as it only stands for  $\sim 60\%$  of the wavefunction.

## INTRODUCTION

For more than three decades, understanding the mechanism of superconductivity observed at high critical temperature (HTC) in strongly correlated cuprates [1] has been the “holy grail” of many theoretical and experimental condensed matter researchers. In this context, the observation of superconductivity in nickelates  $LnNiO_2$ ,  $Ln=\{\text{La, Nd and Pr}\}$  [2–4] upon doping with holes is remarkable. These superconducting nickelates are isostructural as well as isoelectronic to HTC cuprate superconductors and thus enable the comparison of the essential physical features that may be playing a crucial role in the mechanism driving superconductivity.

$LnNiO_2$  family of compounds are synthesized in the so-called infinite-layer structure, where NiO<sub>2</sub> and  $Ln$  layers are stacked alternatively [2]. The NiO<sub>2</sub> planes are identical to the CuO<sub>2</sub> planes in HTC cuprates which host much of the physics leading to superconductivity [5]. A simple valence counting of the these nickelates reveals a 1+ oxidation state for Ni (2- for O and 3+ for  $Ln$ ) with 9 electrons in the  $3d$  manifold. In the cuprates, the Cu<sup>2+</sup> oxidation state gives rise to the same  $3d^9$  electronic configuration. Contrary to many nickel oxides where the Ni atom sits in an octahedral cage of oxygens, in the infinite-layered structure, square planar NiO<sub>4</sub> plaques are formed without the apical oxygens. The crystal field due to square-planar oxygen coordination stabilizes the  $d_{z^2}$  orbital of the  $e_g$  manifold, making its energy close to the  $t_{2g}$  orbitals (the  $3d$  orbitals split to 3-fold  $t_{2g}$  and 2-fold  $e_g$  sub-shells in an octahedral environment). With  $d^9$

occupation, a half-filled  $d_{x^2-y^2}$ -orbital system is realized as in cuprates. In fact, recent resonant inelastic X-ray scattering (RIXS) experiments [6] as well as the *ab initio* correlated multiplet calculations [7] confirm that the Ni<sup>1+</sup>  $d$ - $d$  excitations in NdNiO<sub>2</sub> are similar to the Cu<sup>2+</sup> ions in cuprates [8].

Several electronic structure calculations based on density-functional theory (DFT) have shown that in monovalent nickelates the Ni  $3d_{x^2-y^2}$  states sit at the Fermi energy level [9–11]. These calculations further show that the nickelates are more close to the Mott-Hubbard insulating limit with a decreased Ni  $3d$ -O  $2p$  hybridization compared to cuprates. The latter are considered to be charge transfer insulators [12] where excitations across the electronic band gap involves O  $2p$  to Cu  $3d$  electron transfer. Correlated wavefunction-based calculations [7] indeed find that the contribution from the O  $2p$  hole configuration to the ground state wavefunction in NdNiO<sub>2</sub> is four times smaller than in the cuprate analogue CaCuO<sub>2</sub>. X-ray absorption and photoemission spectroscopy experiments [13, 14] confirm the Mott behavior of nickelates.

In the cuprate charge-transfer insulators, the strong hybridization of the Cu  $3d_{x^2-y^2}$  and O  $2p$  orbitals result in O  $2p$  dominated bonding and Cu  $3d_{x^2-y^2}$ -like antibonding orbitals. As a consequence, the doped holes primarily reside on the bonding O  $2p$  orbitals, making them singly occupied. The unpaired electrons on the Cu  $d_{x^2-y^2}$  and the O  $2p$  are coupled antiferromagnetically resulting in the famous Zhang-Rice (ZR) spin singlet state [15]. In the monovalent nickelates, it is unclear

where the doped-holes reside. Do they form a ZR singlet as in cuprates? Instead, if the holes reside on the Ni site, do they form a high-spin local triplet with two singly occupied Ni  $3d$  orbitals and aligned ferromagnetically or a low-spin singlet with either both the holes residing in the Ni  $3d_{x^2-y^2}$  orbital or two singly occupied Ni  $3d$  but aligned anti-parallel. While Ni L-edge XAS and RIXS measurements [6] conclude that an orbitally polarized singlet state is predominant, where doped holes reside on the Ni  $3d_{x^2-y^2}$  orbital, O K-edge electron energy loss spectroscopy [14] reveal that some of the holes also reside on the O  $2p$  orbitals. On the other hand, calculations based on multi-band  $d-p$  Hubbard models show that the fate of the doped holes is determined by a subtle interplay of Ni onsite ( $U_{dd}$ ), Ni  $d$  - O  $2p$  intersite ( $U_{dp}$ ) Coulomb interactions and the Hund's coupling along with the charge transfer gap [16, 17]. However, with the lack of extensive experimental data, it is difficult to identify the appropriate interaction parameters for a model Hamiltonian study, let alone identifying the model that best describes the physics of superconducting nickelates.

Despite the efforts to discern the similarities and differences between the monovalent nickelates and superconducting cuprates, there is no clear understanding on the nature of doped holes in NdNiO<sub>2</sub>. Particularly, there is no reliable parameter-free *ab initio* analysis of the hole-doped situation. In this work, we investigate the hole-doped ground state in NdNiO<sub>2</sub> and draw parallels to the hole doped ground state of cuprate analogue CaCuO<sub>2</sub>. We use fully *ab initio* many-body wavefunction-based quantum chemistry methodology to compute the ground state wavefunctions for the hole doped NdNiO<sub>2</sub> and CaCuO<sub>2</sub>. We find that the doped hole in NdNiO<sub>2</sub> mainly localizes on the Ni  $3d_{x^2-y^2}$  orbital to form a closed-shell singlet, and this singlet configuration contributes to  $\sim 40\%$  of the wavefunction. In contrast, in CaCuO<sub>2</sub> the Zhang-Rice singlet configurations contribute to  $\sim 65\%$  of the wavefunction. The persistent dynamic radial-type correlations within the Ni  $d$  manifold result in stronger  $d^8$  multiplet effects than in CaCuO<sub>2</sub>, and consequently the additional hole foot-print is more three-dimensional in NdNiO<sub>2</sub>. Our analysis shows that the most commonly used three-band Hubbard model to express the doped scenario in cuprates represents 90% of the  $d^8$  wavefunction for CaCuO<sub>2</sub>, but such a model grossly approximates the  $d^8$  wavefunction for the NdNiO<sub>2</sub> as it only stands for  $\sim 60\%$  of the wavefunction.

In what follows, we first describe the computational methodology we employ in this work where we highlight the novel features of the methods and provide all the computational details. We then present the results of our calculations and conclude with a discussion.

## THE WAVEFUNCTION QUANTUM CHEMISTRY METHOD

*Ab initio* configuration interaction (CI) wavefunction-based quantum chemistry methods, particularly the post Hartree-Fock (HF) complete active space self-consistent field (CASSCF) and the multireference perturbation theory (MRPT), are employed. These methods not only facilitate systematic inclusion of electron correlations, but also enable to quantify different types of correlations, static vs dynamic [18]. These calculations do not use any *ad hoc* parameters to incorporate electron-electron interactions unlike other many-body methods, instead, they are computed fully *ab initio* from the kinetic and Coulomb integrals. Such *ab initio* calculations provide techniques to systematically analyze electron correlation effects and offer insights into the electronic structure of correlated solids that go substantially beyond standard DFT approaches, e.g., see Ref. [7, 19–22] for the  $3d$  TM oxides and Ref. [23–27] for  $5d$  compounds.

### Embedded cluster approach

Since strong electronic correlations are short-ranged in nature [28], a local approach for the calculation of the  $N$  and  $N\pm 1$  -electron wavefunction is a very attractive option for transition metal compounds. In the embedded cluster approach, a finite set of atoms, we call quantum cluster (QC), is cut out from the infinite solid and many-body quantum chemistry methods are used to calculate the electronic structure of the atoms within the QC. The cluster is “embedded” in a potential that accounts for the part of the crystal that is not treated explicitly. In this work, we represent the embedding potential with an array of point charges (PCs) at the lattice positions that are fitted to reproduce the Madelung crystal field in the cluster region [29]. Such procedure enables the use of quantum chemistry calculations for solids involving transition-metal or lanthanide ions, see Refs. [30–32].

### Complete active space self-consistent field

CASSCF method [33] is a specific type of multi-configurational (MC) self-consistent field technique in which a complete set of Slater determinants or configuration state functions (CSFs) is used in the expansion of the CI wavefunction is defined in a constrained orbital space, called the active space. In the CASSCF( $n,m$ ) approach, a subset of  $n$  active electrons are fully correlated among an active set of  $m$  orbitals, leading to a highly multi-configurational (CAS) reference wavefunction. CASSCF method with a properly chosen active space guarantees a qualitatively correct wavefunction for strongly correlated systems where static correlation [33]

effects are taken into account. We consider active spaces as large as CAS(24,30) in this work. Because the conventional CASSCF implementations based on deterministic CI space (the Hilbert space of all possible configurations within the active space) solvers are limited to active spaces of 18 active electrons in 18 orbitals, we use the full configuration interaction quantum Monte Carlo (FCIQMC) [34–36] and density matrix renormalization group (DMRG) theory [37, 38] algorithms to solve the eigenvalue problem defined within the active space.

### Multireference perturbation theory

While the CASSCF calculation provides a qualitatively correct wavefunction, for a quantitative description of a strongly correlated system, dynamic correlations [33] (contributions to the wavefunction from those configurations related to excitations from inactive to active and virtual, and active to virtual orbitals) are also important and must be accounted for. A natural choice is variational multireference CI (MRCI) approach where the CI wavefunction is extended with excitations involving orbitals that are doubly occupied and empty in the reference CASSCF wavefunction [33]. An alternative and computationally less demanding approach to take into account dynamic correlations is based on perturbation theory in second- and higher-orders. In multireference perturbation theory (MRPT) MC zeroth-order wavefunction is employed and excitations to the virtual space are accounted by means of perturbation theory. If the initial choice of the MC wavefunction is good enough to capture the large part of the correlation energy, then the perturbation corrections are typically small. The most common variations of MRPT are the complete active space second-order perturbation theory (CASPT2) [39] and the  $n$ -electron valence second-order perturbation theory (NEVPT2) [40] which differ in the type of zeroth-order Hamiltonian  $H_0$  employed.

### THE *AB INITIO* MODEL

Before we describe the *ab initio* model we consider, let us summarize the widely used and prominent model Hamiltonian to study the nature of doped hole in HTC cuprates and also employed for monovalent nickelates lately. It is the three-band Hubbard model [41] with three orbital degrees of freedom (bands) which include the  $d$  orbital of Cu with  $x^2 - y^2$  symmetry and the in-plane oxygen  $p$  orbitals aligned in the direction of the nearest Cu neighbours. These belong to the  $b_1$  irreducible representation (irrep) of the  $D_{4h}$  point group symmetry realized at the Cu site of the  $\text{CuO}_4$  plaque, the other Cu  $d$  orbitals belong to  $a_1$  ( $d_{z^2}$ ),  $b_2$  ( $d_{xy}$ ) and  $e$  ( $d_{xz,yz}$ ) irreps. The parameters in this Hamiltonian include the

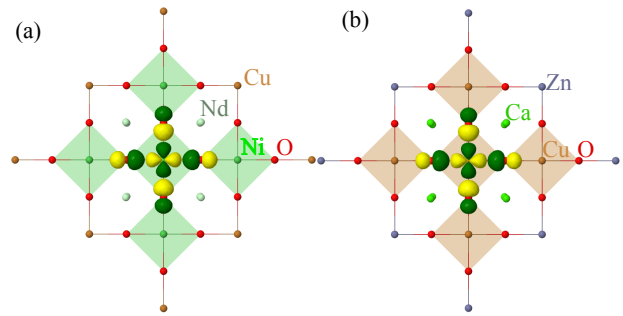


FIG. 1. Quantum cluster of five  $\text{NiO}_4$  (a) and  $\text{CuO}_4$  (b) plaques considered in our calculations. The point-charge embedding is not shown. The symmetry adapted localized  $3d_{x^2-y^2}$  and the oxygen Zhang-Rice-like  $2p$  orbitals, the basis in which the wavefunction in Table III is presented are shown in yellow and green color.

most relevant hopping and Coulomb interactions within this set of orbitals. More recently, the role of the Cu  $3d$  multiplet structure on the hole doped ground state is also studied [42]. While this model explains certain experimental observations, there is still a huge debate on what is the minimum model to describe the low-energy physics of doped cuprates. Nevertheless, this model has also been employed to investigate the character of the doped hole in monovalent nickelates [16, 17, 43].

Within the embedded cluster approach described earlier, we consider a QC of five  $\text{NiO}_4$  ( $\text{CuO}_4$ ) plaques that includes five Ni (Cu) atoms, 16 oxygens and 8 Nd (Ca) atoms. The 10 Ni (Cu) ions neighbouring to the cluster are also included in the QC, however, these are considered as total ion potentials (TIPs). The QC is embedded in point charges that reproduce the electrostatic field of the solid environment. We used the crystal structure parameters for the thin film samples reported in Ref. [2, 44–46].

We used all-electron atomic natural orbital (ANO)-L basis sets of tripple- $\zeta$  quality with additional polarization functions –  $[7s6p4d2f1g]$  for Ni (Cu) [47] and  $[4s3p2d1f]$  for oxygens [48]. For the eight Nd (Ca) atoms large core effective potentials [49–51] and associated  $[3s2p2d]$  basis functions were used. In the case of Nd, the  $f$ -electrons were incorporated in the core.  $\text{Cu}^{1+}$  ( $\text{Zn}^{2+}$ ) total ion potentials (TIPs) with  $[2s1p]$  functions were used for the 10  $\text{Ni}^{1+}$  ( $\text{Cu}^{2+}$ ) [52] [53] neighbouring ions of the QC.

To investigate the role of different interactions in the  $d^8$  ground state, two different active spaces were considered. In the first active space, CAS-1 in Table I, only the orbitals in the  $b_1$  and  $a_1$  irreps are active. These are  $d_{x^2-y^2}$  and  $d_{z^2}$ -like orbitals respectively, and the corresponding double-shell  $4d$  orbitals of each of the five Ni (Cu) atoms. CAS-1 also contains the symmetry-adapted ZR-like composite O  $2p$  and the double-shell  $3p$ -like orbitals, numbers 1-20 and 21-24 in Fig. 2. At the mean-field HF level of

TABLE I. The different active spaces (CAS) considered in this work. NEL is number of active electrons and NORB is the number of active orbitals. The numbers in parenthesis indicate the orbital numbers in Fig 2.

CAS	NEL	NORB
CAS-1	18	24 (1-24)
CAS-2	24	30 (25-30)
CAS-3 <sup>a</sup>	12	14 (1, 6, 11, 16 and 21-30)

<sup>a</sup> The four neighbouring Ni<sup>1+</sup> (Cu<sup>2+</sup>) ions in the quantum cluster are treated as closed shell Cu<sup>1+</sup> (Zn<sup>2+</sup>) ions.

theory, there are 16 electrons within this set of orbitals, resulting in CAS(16,22) active space. In the second active space, CAS-2, orbitals of  $b_2$  and the  $e$  irreps from the central Ni (Cu)  $d$  manifold are also included. These are the  $3d_{xy}$ ,  $3d_{xz,yz}$ -like orbitals and the corresponding  $4d$  orbitals and the six electrons, numbers 25-30 in Fig. 2, resulting in a CAS(24,30) active space. The latter active space takes into account the  $d^8$  multiplet effects within the  $3d$  manifold explicitly.

The two active spaces considered in this work not only describe all the physical effects included in the above mentioned three-band Hubbard model but go beyond. More importantly, we do have any *ad-hoc* input parameters for the calculation as all the physical interactions are implicitly included in the *ab initio* Hamiltonian describing the actual scenario in the real materials. We employed OPENMOLCAS [54] quantum chemistry package for all the calculations.

## RESULTS

### Ground state of the $d^8$ configuration

Starting from the electronic structure of the parent compounds, where each Ni (Cu) is in the  $d^9$  configuration, we compute the electron-removal (in the photoemission terminology)  $d^8$  state to investigate the hole-doped quasiparticle state. Since the parent compounds in  $d^9$  configuration have strong nearest neighbour anti-ferromagnetic (AF) correlations [7], the total spin of our QC in undoped case, with five Ni (Cu) sites, in the AF ground state is  $S_{QC} = 3/2$ . By introducing an additional hole (or removing an electron) from the central Ni (Cu) in our QC, the  $S_{QC}$  values range from 0 to 3. To simplify the analysis of the distribution of the additional hole, we keep the spins on the four neighbouring Ni (Cu) sites parallelly aligned in all our calculations and from now on we only specify the spin multiplicity of the cen-

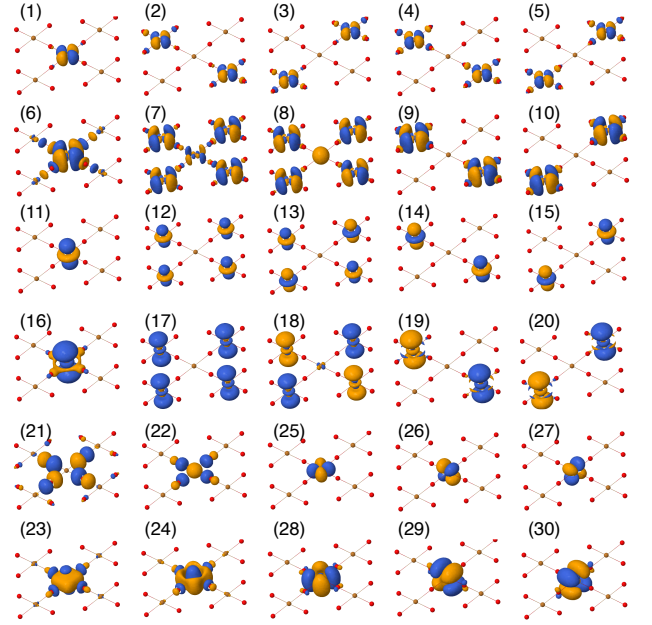


FIG. 2. Active orbital basis used in the CASSCF calculations, plotted using Jmol [55].

tral Ni (Cu)O<sub>4</sub> plaque. The multiplet structure of the  $d^8$  configuration thus consists of only spin singlet and triplet states, spanned by the four irreps of the  $3d$  manifold. The active spaces we consider in this work allow us to compute accurately the excitations only within the  $b_1$  and  $a_1$  irreps [56] and we address the full multiplet structure elsewhere.

When computing the local excitations, a local singlet state on the central Ni (Cu) corresponds to a total spin on the cluster  $S_{QC} = 2$ . However, a local triplet state, with central spin aligned parallel to the neighboring spins, corresponds to  $S_{QC} = 3$  and do not satisfy the AF correlations. To avoid the spin coupling between the central  $d^8$  Ni (Cu) with the neighbouring  $d^9$  Ni (Cu) ions, we replace the latter with closed shell, Cu (Zn)  $d^{10}$ , ions and freeze them at the mean-field HF level. Such a simplification is justified, as the local excitation energy we compute is an order of magnitude larger than the exchange interaction [7].

In Table II, the relative energies of the lowest local spin singlets  $^1A_{1g}$ ,  $^1B_{1g}$  and spin triplet  $^3B_{1g}$  states are shown. These are obtained from CASSCF + CASPT2 calculations with CAS(12,14) active space (CAS-3 in Table I) which includes the  $3d$  and  $4d$  orbitals of the central Ni (Cu) ion and the in-plane O  $2p$  and  $3p$  orbitals in the  $b_1$  irrep. In the CASPT2 calculation, the remaining doubly occupied O  $2p$ , the central Ni (Cu)  $3s$  and  $3p$  orbitals and all the unoccupied virtual orbitals are correlated. It can be seen that the ground state is of  $^1A_{1g}$  symmetry and the lowest triplet excited state, with  $^3B_{1g}$  symmetry, is

TABLE II. Relative energies (in eV) of the electron removal  $d^8$  states in NdNiO<sub>2</sub> and the iso-structural CaCuO<sub>2</sub> obtained from CAS(12,14)SCF and CASSCF+CASPT2 calculations.

State	NdNiO <sub>2</sub>		CaCuO <sub>2</sub>	
	CASSCF	+CASPT2	CASSCF	+CASPT2
$^1A_{1g}$	0.00	0.00	0.00	0.00
$^3B_{1g}$	1.35	1.88	2.26	2.50
$^1B_{1g}$	2.98	3.24	3.21	3.33

around 1.88 eV and 2.5 eV for NdNiO<sub>2</sub> and CaCuO<sub>2</sub> respectively. The AF magnetic exchange in these two compounds is 76 meV and 208 meV respectively [7], and thus we expect that our simplification of making the neighbouring  $d^9$  ions closed shell do not over/underestimate the excitation energies. At the CASSCF level, the  $^1A_{1g}$ - $^3B_{1g}$  excitation energy is 1.35 eV in NdNiO<sub>2</sub> while it is 2.26 eV in CaCuO<sub>2</sub>. Interestingly, the inclusion of dynamical correlations via the CASPT2 calculation, the  $^1A_{1g}$  in NdNiO<sub>2</sub> is stabilized by 0.53 eV compared to  $^3B_{1g}$  state. However, in CaCuO<sub>2</sub>, the  $^1A_{1g}$  state is stabilized by only 0.24 eV. This indicates that the dynamical correlations are more active in the  $^1A_{1g}$  state in NdNiO<sub>2</sub> than in CaCuO<sub>2</sub>. We note that the hole excitations within the 3d orbitals in the irreps  $b_2$  and  $e$ , calculated with this limited active space (CAS-3) results in energies lower than the  $^3B_{1g}$  and  $^1B_{1g}$  states. However, an accurate description of those states requires an enlarged active space that includes not only the same symmetry oxygen 2p and 3p orbitals from the central NiO<sub>4</sub> plaque but also the 3d, 4d manifold of the neighbouring Ni (Cu) ions, making the active space prohibitively large. Here, we concentrate on the analysis of the  $^1A_{1g}$  ground state and address the complete  $d^8$  multiplet spectrum elsewhere.

### Wavefunction of the electron-removal $d^8$ ground state

The  $^1A_{1g}$  ground wavefunction in terms of the weights of the four leading configurations (in the case of CaCuO<sub>2</sub>) is shown in Table III. The wavefunctions corresponding to the CASSCF calculations with the active spaces CAS-1 and CAS-2 are shown. The basis in which the wavefunctions are represented is constructed in two steps: 1) A set of natural orbitals are generated by diagonalising the CASSCF one-body reduced density matrix. 2) To obtain a set of atomic-like symmetry-adapted localized orbital basis, we localize the Ni (Cu) 3d and O 2p orbitals on the central NiO<sub>4</sub> (CuO<sub>4</sub>) plaque through a unitary transformation. Such partial localization within the active space keeps the total energy unchanged. The resulting  $3d_{x^2-y^2}$  and the ZR-like oxygen 2p orbital basis is

shown in Fig 1. FCIQMC calculation was performed in this partial localized basis to obtain the wavefunction as a linear combination of Slater determinants. 10 million walkers were used to converge the FCIQMC energy to within 0.1 mHartree.

From Table III it can be seen that the electron-removal  $d^8$  ground state wavefunction for the two compounds is mostly described by the four configurations spanned by the localized  $3d_{x^2-y^2}$  ( $d_{b_1}$ ) and the symmetry-adapted ZR-like oxygen 2p ( $p_{b_1}$ ) orbitals that are shown in Fig. 1. Let us first discuss the wavefunction obtain from the CAS-1 active space. For NdNiO<sub>2</sub>, the dominant configuration involves two holes on  $3d_{x^2-y^2}$ ,  $|d_{b_1}^\square p_{b_1}^{\uparrow\downarrow}\rangle$ , and contributes to  $\sim 52\%$  of the wavefunction, while the configurations that make up the ZR singlet,  $|d_{b_1}^\uparrow p_{b_1}^\downarrow\rangle$  and  $|d_{b_1}^\downarrow p_{b_1}^\uparrow\rangle$ , contributes to only  $\sim 14\%$ . On the other hand, the  $d^8$   $^1A_{1g}$  state in CaCuO<sub>2</sub> is predominantly the ZR singlet with  $\sim 68\%$  weight. In the CASSCF calculation with CAS-2 active space, where all the electrons in the 3d manifold are explicitly correlated, we find that the character of the wavefunction remains unchanged in NdNiO<sub>2</sub> but weight on the dominant configurations is slightly reduced. On the other hand, in CaCuO<sub>2</sub>, while the contribution from the ZR singlet is slightly reduced, the contribution from  $|d_{b_1}^\square p_{b_1}^{\uparrow\downarrow}\rangle$  configuration is dramatically increased at the expense of the weight on  $|d_{b_1}^\downarrow p_{b_1}^\square\rangle$ . This demonstrates that the additional freedom provided by the  $d_{xy}$  and  $d_{xz/yz}$  orbitals for the electron correlation helps to accommodate the additional hole on the Cu ion.

We note that the four configurations shown in Table III encompass almost 90% of the  $d^8$  wavefunction (with CAS-2 active space) in CaCuO<sub>2</sub>. Thus, the use of a three-band Hubbard model [41, 42] to investigate the role of doped holes in CuO<sub>2</sub> planes is a reasonable

TABLE III. Ni and Cu  $3d^8$   $^1A_{1g}$  ground state wavefunction: Weights (%) of the leading configurations in the wavefunction computed for NdNiO<sub>2</sub> and CaCuO<sub>2</sub> with active spaces CAS-1 and CAS-2 (see Table I).  $d_{b_1}$  and  $p_{b_1}$  are the localized Ni (Cu)  $3d_{x^2-y^2}$  and the oxygen 2p ZR-like orbitals (see Fig. 1) in the  $b_1$  irrep respectively. Arrows in the superscript indicate the spin of the electrons and a  $\square$  indicates two holes.

$^1A_{1g}$	NdNiO <sub>2</sub>		CaCuO <sub>2</sub>	
	CAS-1	CAS-2	CAS-1	CAS-2
$ d_{b_1}^\square p_{b_1}^{\uparrow\downarrow}\rangle$	51.87	42.40	4.20	20.25
$ d_{b_1}^\uparrow p_{b_1}^\downarrow\rangle$	8.27	10.48	42.58	38.52
$ d_{b_1}^\downarrow p_{b_1}^\uparrow\rangle$	6.07	7.60	25.00	25.60
$ d_{b_1}^{\uparrow\downarrow} p_{b_1}^\square\rangle$	0.09	0.23	21.56	5.14

choice. However, for NdNiO<sub>2</sub> these configurations cover only 60% of the  $d^8$  wavefunction, hence a three-band Hubbard model is too simple to describe the hole-doped monovalent nickelates.

A more intuitive and visual understanding of the distribution of the additional hole can be obtained by plotting the difference of the  $d^8$  and the  $d^9$  ground state electron densities as shown in Fig. 3. Electron density of a multi-configurational state can be computed as a sum of densities arising from the natural orbitals and corresponding (well-defined) occupation numbers. We used Multiwfn program [57] to perform this summation. The negative values of the heat map of the electron density difference (blue color) and the positive values (in red) represent respectively the extra hole density and additional electron density in  $d^8$  state compared to the  $d^9$  state. From Fig. 3(a)/(c) that show the density difference in the NiO<sub>2</sub>/CuO<sub>2</sub> planes (xy-plane), we conclude the following:

1. The hole density is concentrated on the Ni site (darker blue) with  $b_1$  ( $d_{x^2-y^2}$ ) symmetry in NdNiO<sub>2</sub> whereas it is distributed evenly on the four oxygen and the central Cu ions with  $b_1$  symmetry in CaCuO<sub>2</sub>, a result consistent with the wavefunction reported in Table III.
2. In NdNiO<sub>2</sub>, the hole density is spread out around the Ni ion with larger radius, and otherwise in CaCuO<sub>2</sub>. This demonstrates that the 3d manifold in Cu is much more localized than in Ni and therefore the onsite Coulomb repulsion  $U$  is comparatively smaller for Ni.
3. The darker red regions around the Ni site in NdNiO<sub>2</sub> indicate stronger  $d^8$  multiplet effects that result in rearrangement of electron density compared to  $d^9$  configuration.
4. In CaCuO<sub>2</sub>, we see darker red regions on the oxygen ions instead, which shows that the significant presence of a hole on these ions results in noticeable electron redistribution.

The electron density difference in the xz-plane (which is perpendicular to the NiO<sub>2</sub>/CuO<sub>2</sub> planes) is quite different in the two compounds. The hole density in NdNiO<sub>2</sub> is spread out up to 2 Å in the  $z$ -direction, unlike in CaCuO<sub>2</sub>, where it is confined to within 1 Å. We attribute this to the strong radial-type correlations in NdNiO<sub>2</sub>. With the creation of additional hole on the  $3d_{x^2-y^2}$  orbital, the electron density which is spread out in the  $d_{z^2}$  symmetry via the dynamical correlation between  $3d_{z^2}$  and  $4d_{z^2}$  orbitals [7], becomes more compact in the  $d_{z^2}$  symmetry through the reverse breathing. Thus, we see a strong red region with  $3d_{z^2}$  profile and a blue region with expanded  $4d_{z^2}$  profile.

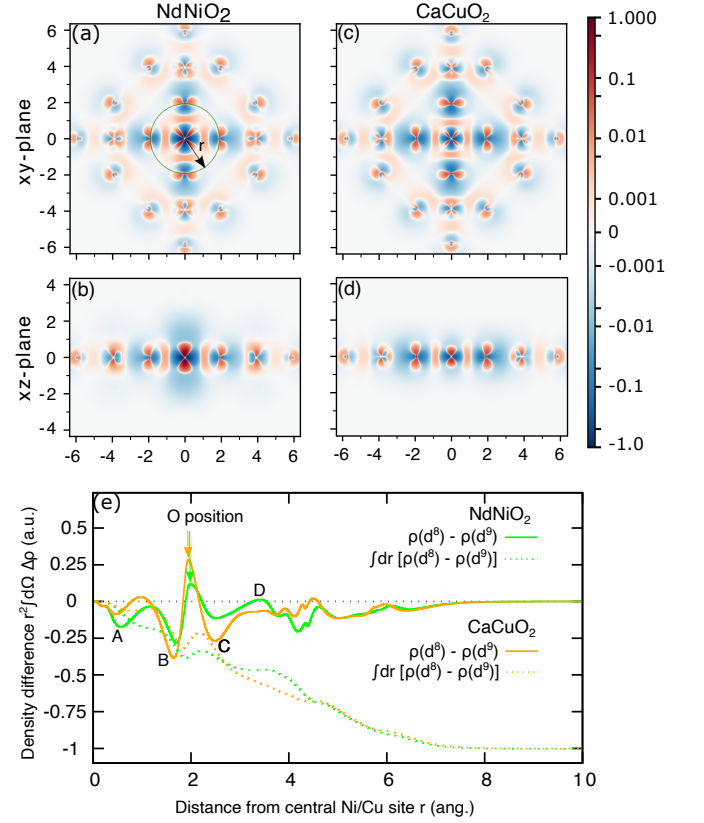


FIG. 3. Electron density difference of the  $d^8$  and  $d^9$  ground states ( $\rho(d^8) - \rho(d^9)$ ) for NdNiO<sub>2</sub> in the xy-plane (a) and xz-plane (b), and for CaCuO<sub>2</sub> xy-plane (c) and xz-plane (d). The coordinates of the central Ni (Cu)  $d^8$  ion are set to (0,0). The scale of the heat-bar is logarithmic between  $\pm 0.001$  to  $\pm 1.0$  and is linear between 0 and  $\pm 0.001$ . (e) Electron density difference integrated over a sphere centered on the central Ni(Cu) atoms (full curves) as a function of the radius  $r$  shown in (a). The result of an additional radial integration (dashed curves) as a function of the upper integration limit.

To obtain a quantitative understanding of the charge density differences for the two compounds, in Fig. 3(e) we plot the electron density difference integrated over a sphere centered on the central Ni(Cu) atom as a function of the radius  $r$  shown in Fig. 3(a). Four features, which we marked A-D, clearly demonstrate the contrast in the charge density differences in the two compounds. From the feature A at  $r$  close to Ni (Cu), it is evident that the extent of hole density around Ni in NdNiO<sub>2</sub> is larger than around Cu in CaCuO<sub>2</sub>. The features B and C that are on either side of the position of oxygen ions show that the hole density is significantly larger on oxygen atoms in CaCuO<sub>2</sub> than in the NdNiO<sub>2</sub>. It is interesting to note that we see a jump (feature D) in the electron density above zero at  $r$  close to the position of Nd ions in NdNiO<sub>2</sub>, while in CaCuO<sub>2</sub> the curve is flat in the region of Ca ions. This shows that there is some electron redistribution happening around the Nd ions.



The hole density within a solid sphere (SS) around the central Ni (Cu) atom obtained by additional integration over the radius  $r$  is also shown in Fig. 3(e) with dashed curves. It can be seen that the total hole density within the SS of  $r \sim 4 \text{ \AA}$ , where the neighboring Ni (Cu) ions are located, is only  $\sim 0.5$  in both the compounds, with slight differences related to the feature D. This is due to the screening of the hole with the electron density pulled in from the farther surroundings. As one would expect, a SS with  $r$  of the size of the cluster, the total hole density is one in both the compounds.

### Orbital entanglement entropy

To analyse the different type of correlations active in the two compounds in  $d^8$  configuration, we compute the entanglement entropy [58–60]. While the single orbital entropy,  $s(1)_i$ , quantifies the correlation between  $i$ -th orbital and the remaining set of orbitals, the mutual information,  $I_{i,j}$  is the two-orbital entropy between  $i$  and  $j$  [61, 62], and illustrates the correlation of an orbital with another, in the embedded environment comprising of all other orbitals. We used QCMAQUIS [63] embedded in OPENMOLCAS [54] package to compute the entropies.

In Figure 4,  $s(1)_i$  and  $I_{i,j}$  extracted from CASSCF calculations with CAS-2 active space for NdNiO<sub>2</sub> and CaCuO<sub>2</sub> are shown. The orbital basis for which the entropy is computed is the same as the basis in which the wavefunction presented in Table III is expanded. As mentioned previously, this orbital basis is obtained from par-

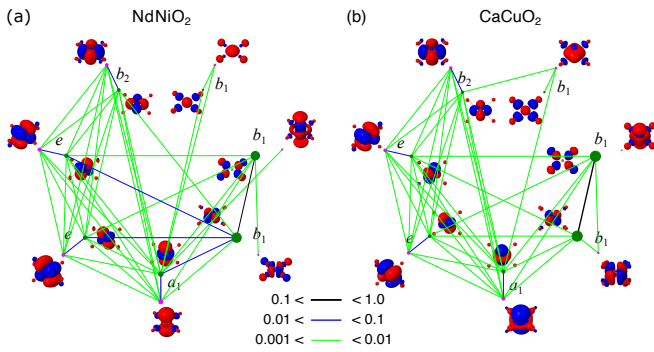


FIG. 4. Single orbital entanglement entropy,  $s(1)_i$ , (dots) and mutual orbital entanglement entropy,  $I_{i,j}$ , (colored lines) of the orbital basis used to expand the  $d^8$  wavefunction in Table III for NdNiO<sub>2</sub> (a) and CaCuO<sub>2</sub> (b). Entanglement entropy of the orbitals centred on the central NiO<sub>4</sub>/CuO<sub>4</sub> plaque are only shown. The irrep to which the orbitals belong to are also shown. The green and magenta colors represent the two different set of orbitals, occupied (at the HF level) and the corresponding double-shell (virtual), respectively. The thickness of the black, blue and green lines denote the strength of  $I_{i,j}$ , and the size of the dots is proportional to  $s(1)_i$ .

tial localization of the natural orbitals in a way that only the  $3d_{x^2-y^2}$  and the O  $2p$  ZR-like orbitals are localized. Since a large part of electron correlation is compressed in natural orbitals, we see a tiny  $s(1)_i$  for all orbitals except for the localized  $3d_{x^2-y^2}$  and the O  $2p$  ZR-like orbitals where it is significant. This is consistent with the wavefunction in Table III. The mutual orbital entanglement between pairs of orbitals shows strong entanglement between the  $3d_{x^2-y^2}$  and the O  $2p$  ZR-like orbitals for both NdNiO<sub>2</sub> and CaCuO<sub>2</sub>, a consequence of the dominant weight of the configurations spanned by these two orbitals in the wavefunction. The next strongest entanglement is between the Ni/Cu  $3d$  valence and their double-shell  $4d$  orbitals. Such strong entanglement also observed for the undoped  $d^9$  ground state [7], is a result of dynamical radial correlation [18] and orbital breathing effects [64, 65]. Interestingly, the entanglement entropy in the range 0.001-0.01 (green lines) is quite similar in the two compounds, although one sees more entanglement connections in NdNiO<sub>2</sub>. A comparison of the entropy information between NdNiO<sub>2</sub> and CaCuO<sub>2</sub> reveals that the Ni  $3d$  and  $4d$ -like orbitals contribute rather significantly (thicker blue lines) to the total entropy, in contrast to the Cu  $3d$  and  $4d$ -like orbitals, something that is also seen in the undoped compounds [7].

### CONCLUSIONS AND DISCUSSION

In conclusion, our *ab initio* many-body quantum chemistry calculations for the electron removal ( $d^8$ ) states find a low-spin closed-shell singlet ground state in NdNiO<sub>2</sub> and that the additional hole is mainly localized on the Ni  $3d_{x^2-y^2}$  orbital, unlike in CaCuO<sub>2</sub>, where a Zhang-Rice singlet is predominant. We emphasise that the  $d^8$  wavefunction is highly multi-configurational where the dominant closed-shell singlet configuration weight is only  $\sim 42\%$ . This result is consistent with the experimental evidence [6, 14] of orbitally polarized singlet state as well as the presence of holes on the O  $2p$  orbitals. Importantly, the persistent dynamic radial-type correlations within the Ni  $d$  manifold result in stronger  $d^8$  multiplet effects in NdNiO<sub>2</sub>, and consequently the additional hole foot-print is more three dimensional. In CaCuO<sub>2</sub>, we find that the electron correlations within the  $d_{xy}$  and  $d_{xz/yz}$  orbitals changes the hole-doped wavefunction significantly. Specifically, the double hole occupation of Cu  $d_{x^2-y^2}$  is significantly increased and this can influence the transport properties.

It was recently proposed that nickelates could be a legitimate realization of the single-band Hubbard model [66]. However, our analysis shows that even the three-band Hubbard model [67], which successfully describes the hole-doped scenario in cuprates, falls short to describe hole-doped nickelates and additional orbital degrees of freedom are indeed necessary for the descrip-

tion of the strong multiplet effects we find. Much has been discussed about the importance of rare-earth atoms for the electronic structure of superconducting nickelates, e.g. see [68]. The three-dimensional nature of the hole density we find in NdNiO<sub>2</sub> might also be hinting at the importance of out-of-plane Nd ions. It would be interesting to compare the hole density of NdNiO<sub>2</sub> with other isostructural nickelates such as LaNiO<sub>2</sub> where La 5d states are far from the Fermi energy. Since the infinite-layered monovalent nickelates are thin films and often grown on substrates, one could ask the question of how the electronic structure of the undoped and doped compounds changes with varying Ni-O bond length. Would this influence the role of electronic correlations in  $d^9$  nickelates? We will address these in the near future.

### CONFLICT OF INTEREST STATEMENT

The authors express no conflict of interests.

### AUTHOR CONTRIBUTIONS

VMK and AA designed the project. VMK and NAB performed the calculations. All the authors analysed the data. VMK wrote the paper with inputs from NAB and AA.

### FUNDING

We gratefully acknowledge the Max Plank Society for financial support.

### ACKNOWLEDGMENTS

VMK would like to acknowledge Giovanni Li Manni and Oskar Weser for fruitful discussions.

---

\* V.Katukuri@fkf.mpg.de

† A.Alavi@fkf.mpg.de

- [1] J. G. Bednorz and K. A. Müller. Possible high T-c superconductivity in the Ba-La-Cu-O system. *Z. Phys. B*, 64:189, 1986.
- [2] Danfeng Li, Kyuho Lee, Bai Yang Wang, Motoki Osada, Samuel Crossley, Hye Ryoung Lee, Yi Cui, Yasuyuki Hikita, and Harold Y. Hwang. Superconductivity in an infinite-layer nickelate. *Nature*, 572(7771):624–627, August 2019.
- [3] Motoki Osada, Bai Yang Wang, Berit H. Goodge, Kyuho Lee, Hyeok Yoon, Keita Sakuma, Danfeng Li, Masashi Miura, Lena F. Kourkoutis, and Harold Y. Hwang. A Superconducting Praseodymium Nickelate with Infinite Layer Structure. *Nano Lett.*, page 0c01392, 2020.
- [4] Motoki Osada, Bai Yang Wang, Berit H. Goodge, Shannon P. Harvey, Kyuho Lee, Danfeng Li, Lena F. Kourkoutis, and Harold Y. Hwang. Nickelate Superconductivity without Rare-Earth Magnetism: (La,Sr)NiO<sub>2</sub>. *Adv. Mater.*, page 2104083, September 2021.
- [5] B. Keimer, S. A. Kivelson, M. R. Norman, S. Uchida, and J. Zaanen. From quantum matter to high-temperature superconductivity in copper oxides. *Nature*, 518(7538):179–186, February 2015.
- [6] M. Rossi, H. Lu, A. Nag, D. Li, M. Osada, K. Lee, B. Y. Wang, S. Agrestini, M. Garcia-Fernandez, Y. D. Chuang, Z. X. Shen, H. Y. Hwang, B. Moritz, Ke-Jin Zhou, T. P. Devereaux, and W. S. Lee. Orbital and Spin Character of Doped Carriers in Infinite-Layer Nickelates. 2020.
- [7] Vamshi M. Katukuri, Nikolay A. Bogdanov, Oskar Weser, Jeroen van den Brink, and Ali Alavi. Electronic correlations and magnetic interactions in infinite-layer NdNiO<sub>2</sub>. *Phys. Rev. B*, 102(24):241112, 2020.
- [8] M Moretti Sala, V Bisogni, C Aruta, G Balestrino, H Berger, N B Brookes, G M de Luca, D Di Castro, M Grioni, M Guarise, P G Medaglia, F Miletto Granozio, M Minola, P Perna, M Radovic, M Salluzzo, T Schmitt, K J Zhou, L Braicovich, and G Ghiringhelli. Energy and symmetry of dd excitations in undoped layered cuprates measured by Cu L<sub>3</sub> resonant inelastic x-ray scattering. *New J. Phys.*, 13(4):043026, 2011.
- [9] K.-W. Lee and W. E. Pickett. Infinite-layer LaNiO<sub>2</sub> : Ni<sup>1+</sup> is not Cu<sup>2+</sup>. *Phys. Rev. B*, 70(16):165109, October 2004.
- [10] Zhao Liu, Zhi Ren, Wei Zhu, Zhengfei Wang, and Jinlong Yang. Electronic and magnetic structure of infinite-layer NdNiO<sub>2</sub>: trace of antiferromagnetic metal. *npj Quantum Mater.*, 5(1):31, December 2020.
- [11] Hu Zhang, Lipeng Jin, Shanmin Wang, Bin Xi, Xingqiang Shi, Fei Ye, and Jia-Wei Mei. Effective Hamiltonian for nickelate oxides Nd<sub>1-x</sub>Sr<sub>x</sub>NiO<sub>2</sub>. *Phys. Rev. Research*, 2:013214, Feb 2020.
- [12] J. Zaanen, G. A. Sawatzky, and J. W. Allen. Band gaps and electronic structure of transition-metal compounds. *Phys. Rev. Lett.*, 55:418–421, Jul 1985.
- [13] M. Hepting, D. Li, C.J. Jia, H. Lu, E. Paris, Y. Tseng, X. Feng, M. Osada, E. Been, Y. Hikita, Y.D. Chuang, Z. Hussain, K.J. Zhou, A. Nag, M. Garcia-Fernandez, M. Rossi, H.Y. Huang, D.J. Huang, Z.X. Shen, T. Schmitt, H.Y. Hwang, B. Moritz, J. Zaanen, T.P. Devereaux, and W.S. Lee. Electronic structure of the parent compound of superconducting infinite-layer nickelates. *Nature Materials*, 19(4):381–385, 2020.
- [14] Berit H. Goodge, Danfeng Li, Kyuho Lee, Motoki Osada, Bai Yang Wang, George A. Sawatzky, Harold Y. Hwang, and Lena F. Kourkoutis. Doping evolution of the Mott–Hubbard landscape in infinite-layer nickelates. *Proceedings of the National Academy of Sciences*, 118(2), 2021.
- [15] F. C. Zhang and T. M. Rice. Effective Hamiltonian for the superconducting Cu oxides. *Phys. Rev. B*, 37(7):3759–3761, 1988.
- [16] Mi Jiang, Mona Berciu, and George A. Sawatzky. Critical Nature of the Ni Spin State in Doped NdNiO<sub>2</sub>. *Phys. Rev. Lett.*, 124:207004, May 2020.
- [17] Tharathep Plienbumrung, Michael Thobias Schmid, Maria Daghofer, and Andrzej M. Oleś. Character of



- Doped Holes in  $\text{Nd}_{1-x}\text{Sr}_x\text{NiO}_2$ . *Condensed Matter*, 6(3):33, 2021.
- [18] T. Helgaker, P. Jørgensen, and J. Olsen. *Molecular electronic-structure theory*. Wiley, Chichester, 2000.
  - [19] D. Muñoz, F. Illas, and I. de P. R. Moreira. Accurate Prediction of Large Antiferromagnetic Interactions in High- $T_c$   $\text{HgBa}_2\text{Ca}_{n-1}\text{Cu}_n\text{O}_{2n+2+\delta}$  ( $n=2,3$ ) Superconductor Parent Compounds. *Phys. Rev. Lett.*, 84:1579–1582, Feb 2000.
  - [20] L. Hozoi, L. Siurakshina, P. Fulde, and J. van den Brink. Ab initio determination of Cu 3d orbital energies in layered copper oxides. *Sci. Rep.*, 1:65, 2011.
  - [21] L. Hozoi and P. Fulde. *Computational Methods for Large Systems: Electronic Structure Approaches for Biotechnology and Nanotechnology*. John Wiley & Sons, Hoboken, 2011.
  - [22] N. A. Bogdanov, J. van den Brink, and L. Hozoi. Ab initio computation of  $d$ - $d$  excitation energies in low-dimensional Ti and V oxychlorides. *Phys. Rev. B*, 84:6, Dec 2011.
  - [23] Vamshi M. Katukuri, Hermann Stoll, Jeroen van den Brink, and Liviu Hozoi. Ab initio determination of excitation energies and magnetic couplings in correlated quasi-two-dimensional iridates. *Phys. Rev. B*, 85:220402, 2012.
  - [24] Nikolay A. Bogdanov, Rémi Maurice, Ioannis Rousochatzakis, Jeroen van den Brink, and Liviu Hozoi. Magnetic state of pyrochlore  $\text{Cd}_2\text{Os}_2\text{O}_7$  emerging from strong competition of ligand distortions and longer-range crystalline anisotropy. *Phys. Rev. Lett.*, 110:127206, 2013.
  - [25] H. Gretarsson, J. P. Clancy, X. Liu, J. P. Hill, Emil Bozin, Yogesh Singh, S. Manni, P. Gegenwart, Jungho Kim, A. H. Said, D. Casa, T. Gog, M. H. Upton, Heung-Sik Kim, J. Yu, Vamshi M. Katukuri, L. Hozoi, J. van den Brink, and Young-June Kim. Crystal-field splitting and correlation effect on the electronic structure of  $\text{A}_2\text{IrO}_3$ . *Phys. Rev. Lett.*, 110:076402, 2013.
  - [26] Vamshi M. Katukuri, Viktor Yushankhai, Liudmila Siurakshina, Jeroen van den Brink, Liviu Hozoi, and Ioannis Rousochatzakis. Mechanism of basal-plane antiferromagnetism in the spin-orbit driven iridate  $\text{Ba}_2\text{IrO}_4$ . *Phys. Rev. X*, 4:021051, Jun 2014.
  - [27] V. M. Katukuri, S. Nishimoto, V. Yushankhai, A. Stoyanova, H. Kandpal, S. Choi, R. Coldea, I. Rousochatzakis, L. Hozoi, and J. van den Brink. Kitaev interactions between  $j = 1/2$  moments in honeycomb  $\text{Na}_2\text{IrO}_3$  are large and ferromagnetic: insights from ab initio quantum chemistry calculations. *New J. Phys.*, 16(1):013056, 2014.
  - [28] P. Fulde. *Correlated Electrons in Quantum Matter*. World Scientific, 2012.
  - [29] M. Klintonberg, S.E. Derenzo, and M.J. Weber. Accurate crystal fields for embedded cluster calculations. *Comp. Phys. Comm.*, 131:120, 2000.
  - [30] Vamshi M. Katukuri, Hermann Stoll, Jeroen van den Brink, and Liviu Hozoi. Ab initio determination of excitation energies and magnetic couplings in correlated quasi-two-dimensional iridates. *Phys. Rev. B*, 85(22):220402, June 2012.
  - [31] Vamshi M. Katukuri, Karla Roszeitis, Viktor Yushankhai, Alexander Mitrushchenkov, Hermann Stoll, Michel van Veenendaal, Peter Fulde, Jeroen van den Brink, and Liviu Hozoi. Electronic Structure of Low-Dimensional  $4d^5$  Oxides: Interplay of Ligand Distortions, Overall Lattice Anisotropy, and Spin-Orbit Interactions. *Inorg. Chem.*, 53(10):4833–4839, May 2014.
  - [32] P. Babkevich, Vamshi M. Katukuri, B. Fåk, S. Rols, T. Fennell, D. Pajić, H. Tanaka, T. Pardini, R. R. P. Singh, A. Mitrushchenkov, O. V. Yazyev, and H. M. Rønnow. Magnetic Excitations and Electronic Interactions in  $\text{Sr}_2\text{CuTeO}_6$ : A Spin-1/2 Square Lattice Heisenberg Antiferromagnet. *Phys. Rev. Lett.*, 117(23):237203, December 2016.
  - [33] T. Helgaker, P. Jørgensen, and J. Olsen. *Molecular Electronic-Structure Theory*. Wiley, Chichester, 2000.
  - [34] George H. Booth, Alex J. W. Thom, and Ali Alavi. Fermion Monte Carlo without fixed nodes: a game of life, death, and annihilation in Slater determinant space. *J. Chem. Phys.*, 131(5):054106, 2009.
  - [35] Deidre Cleland, George H. Booth, and Ali Alavi. Survival of the fittest: Accelerating convergence in full configuration-interaction quantum Monte Carlo. *J. Chem. Phys.*, 132(4):041103, January 2010.
  - [36] K. Guthrie, R. J. Anderson, N. S. Blunt, N. A. Bogdanov, D. Cleland, D. Dattani, W. Dobbrautz, K. Ghanem, P. Jeszenski, N. Liebermann, G. Li Manni, A. Y. Lozovoi, H. Luo, D. Ma, F. Merz, C. Overy, M. Rampp, P. K. Samanta, L. R. Schwarz, J. J. Shepherd, S. D. Smart, E. Vitale, O. Weser, G. H. Booth, and A. Alavi. NECI:  $N$ -Electron Configuration Interaction with an emphasis on state-of-the-art stochastic methods. *J. Chem. Phys.*, 2020, under review.
  - [37] Garnet Kin-Lic Chan and Sandeep Sharma. The Density Matrix Renormalization Group in Quantum Chemistry. *Ann. Rev. Phys. Chem.*, 62(1):465–481, 2011.
  - [38] Sandeep Sharma and Garnet Kin-Lic Chan. Spin-adapted density matrix renormalization group algorithms for quantum chemistry. *J. Chem. Phys.*, 136(12):124121, March 2012.
  - [39] Kerstin Andersson, Per-Åke Malmqvist, and Björn O. Roos. Second-order perturbation theory with a complete active space self-consistent field reference function. *J. Chem. Phys.*, 96(2):1218–1226, 1992.
  - [40] C. Angeli, R. Cimiraglia, S. Evangelisti, T. Leininger, and J.-P. Malrieu. Introduction of  $n$ -electron valence states for multireference perturbation theory. *J. Chem. Phys.*, 114(23):10252–10264, June 2001.
  - [41] V. J. Emery. Theory of high- $T_c$  superconductivity in oxides. *Phys. Rev. Lett.*, 58:2794–2797, Jun 1987.
  - [42] Mi Jiang, Mirko Moeller, Mona Berciu, and George A. Sawatzky. Relevance of Cu  $-3d$  multiplet structure in models of high- $T_c$  cuprates. *Phys. Rev. B*, 101:035151, Jan 2020.
  - [43] Tharathep Plienbumrung, Maria Daghofer, and Andrzej M. Oleś. Interplay between Zhang-Rice singlets and high-spin states in a model for doped  $\text{NiO}_2$  planes. *Phys. Rev. B*, 103:104513, Mar 2021.
  - [44] M.A. Hayward and M.J. Rosseinsky. Synthesis of the infinite layer Ni(I) phase  $\text{NdNiO}_{2+x}$  by low temperature reduction of  $\text{NdNiO}_3$  with sodium hydride. *Solid State Sci.*, 5(6):839–850, June 2003.
  - [45] Naoya Kobayashi, Zenji Hiroi, and Mikio Takano. Compounds and Phase Relations in the  $\text{SrO-CaO-CuO}$  System under High Pressure. *J. Solid State Chem.*, 132(2):274–283, 1997.
  - [46] J. Karpinski, I. Mangelschots, H. Schwer, K. Conder, A. Morawski, T. Lada, and A. Paszewin. Single crys-

- tal growth of HgBaCaCuO and infinite layer CaCuO<sub>2</sub> at high gas pressure. *Physica C*, 235-240:917–918, 1994.
- [47] Björn O. Roos, Roland Lindh, P. Malmqvist, Valera Veryazov, and P. Widmark. New Relativistic ANO Basis Sets for Transition Metal Atoms. *J. Phys. Chem. A*, 109(29):6575–6579, July 2005.
- [48] Björn O. Roos, Roland Lindh, P. Malmqvist, Valera Veryazov, and P. Widmark. Main Group Atoms and Dimers Studied with a New Relativistic ANO Basis Set. *J. Phys. Chem. A*, 108(15):2851–2858, April 2004.
- [49] M. Dolg, H. Stoll, A. Savin, and H. Preuss. Energy-adjusted pseudopotentials for the rare earth elements. *Theor. Chim. Acta*, 75(3):173–194, 1989.
- [50] M. Dolg, H. Stoll, and H. Preuss. A combination of quasirelativistic pseudopotential and ligand field calculations for lanthanoid compounds. *Theor. Chim. Acta*, 85(6):441–450, June 1993.
- [51] M. Kaupp, P. v. R. Schleyer, H. Stoll, and H. Preuss. Pseudopotential approaches to Ca, Sr, and Ba hydrides. Why are some alkaline earth MX<sub>2</sub> compounds bent? *J. Chem. Phys.*, 94(2):1360–1366, January 1991.
- [52] Gudrun Igel-Mann. *Semiempirische Pseudopotentiale: Untersuchungen an Hauptgruppenelementen und Nebengruppenelementen mit abgeschlossener d-Schale*. PhD thesis, Stuttgart, Univ., Stuttgart, 1987.
- [53] Energy-consistent Pseudopotentials of Stuttgart/Cologne group, <http://www.tc.uni-koeln.de/cgi-bin/pp.pl?language=en,format=molpro,element=Zn,job=getecp,ecp=ECP28SDF>, [Accessed: 15-Sept-2021].
- [54] Ignacio Fdez. Galván, Morgane Vacher, Ali Alavi, Celestino Angeli, Francesco Aquilante, Jochen Autschbach, Jie J. Bao, Sergey I. Bokarev, Nikolay A. Bogdanov, Rebecca K. Carlson, Liviu F. Chibotaru, Joel Creutzberg, Nike Dattani, Mickaël G. Delcey, Sijia S. Dong, Andreas Dreuw, Leon Freitag, Luis Manuel Frutos, Laura Gagliardi, Frédéric Gendron, Angelo Giussani, Leticia González, Gilbert Grell, Meiyuan Guo, Chad E. Hoyer, Marcus Johansson, Sebastian Keller, Stefan Knecht, Goran Kovačević, Erik Källman, Giovanni Li Manni, Marcus Lundberg, Yingjin Ma, Sebastian Mai, João Pedro Malhado, PerÅke Malmqvist, Philipp Marquetand, Stefanie A. Mewes, Jesper Norell, Massimo Olivucci, Markus Oppel, Quan Manh Phung, Kristine Pierloot, Felix Plasser, Markus Reiher, Andrew M. Sand, Igor Schapiro, Prachi Sharma, Christopher J. Stein, Lasse Kragh Sørensen, Donald G. Truhlar, Mihkel Ugandi, Liviu Ungur, Alessio Valentini, Steven Vancoillie, Valera Veryazov, Oskar Weser, Tomasz A. Wesolowski, Per-Olof Widmark, Sebastian Wouters, Alexander Zech, J. Patrick Zobel, and Roland Lindh. OpenMolcas: From Source Code to Insight. *J. Chem. Theory Comput.*, 15(11):5925–5964, November 2019.
- [55] Jmol development team. Jmol.
- [56] For an accurate quantitative description of the multiplet structure spanned by the other two irreps  $b_1$  and  $e$ , one would need to extend the active space and include the  $3d$  and  $4d$  manifolds of the four neighbouring Ni (Cu) atoms as well as the O  $2p$  orbitals of the same symmetry, resulting in a gigantic 68 electrons in 74 orbitals active space.
- [57] Tian Lu and Feiwu Chen. Multiwfn: A multifunctional wavefunction analyzer. *J. Comput. Chem.*, 33(5):580–592, 2012.
- [58] Katharina Boguslawski, Paweł Tecmer, Örs Legeza, and Markus Reiher. Entanglement Measures for Single and Multireference Correlation Effects. *J. Phys. Chem. Lett.*, 3(21):3129–3135, November 2012.
- [59] Katharina Boguslawski, Paweł Tecmer, Gergely Barcza, Örs Legeza, and Markus Reiher. Orbital Entanglement in Bond-Formation Processes. *J. Chem. Theory Comput.*, 9(7):2959–2973, July 2013.
- [60] Katharina Boguslawski and Paweł Tecmer. Orbital entanglement in quantum chemistry. *Int. J. Quantum Chem.*, 115(19):1289–1295, October 2015.
- [61] J. Legeza and J. Sólyom. Optimizing the density-matrix renormalization group method using quantum information entropy. *Phys. Rev. B*, 68(19):195116, November 2003.
- [62] Jörg Rissler, Reinhard M. Noack, and Steven R. White. Measuring orbital interaction using quantum information theory. *Chemical Physics*, 323(2-3):519–531, April 2006.
- [63] Sebastian Keller, Michele Dolfi, Matthias Troyer, and Markus Reiher. An efficient matrix product operator representation of the quantum chemical Hamiltonian. *J. Chem. Phys.*, 143(24):244118, 2015.
- [64] O. Gunnarsson, O. K. Andersen, O. Jepsen, and J. Zaanen. Density-functional calculation of the parameters in the Anderson model: Application to Mn in CdTe. *Phys. Rev. B*, 39:1708, 1989.
- [65] N. A. Bogdanov, G. Li Manni, S. Sharma, O. Gunnarsson, and A. Alavi. Superconductivity in infinite-layer nickelates. *Nat. Phys.*, 2021.
- [66] Motoharu Kitatani, Liang Si, Oleg Janson, Ryotaro Arita, Zhicheng Zhong, and Karsten Held. Nickelate superconductors – a renaissance of the one-band Hubbard model. *npj Quantum Materials*, (5):59, 2020.
- [67] H. Eskes and G.A. Sawatzky. Single- and triple-, or, multiple-band Hubbard models. *Phys. Rev. B*, 44:9656–9666.
- [68] Yusuke Nomura and Ryotaro Arita. Superconductivity in infinite-layer nickelates. 2021.